CHARACTERISTICS OF MEASURED 4X4 AND 10X10 MIMO WIRELESS CHANNEL DATA AT 2.4-GHZ

Jon W. Wallace and Michael A. Jensen*

Brigham Young University
Electrical and Computer Engineering Dept.
459 CB, Provo, UT 84602
wallacej@et.byu.edu, jensen@ee.byu.edu

1. INTRODUCTION

Recent work has demonstrated theoretical increases in capacity in a multipath-rich environment when multiple antennas are used on both sides of the link [1]. These studies generally rely on simple analytical models for the multiple-input multiple-output (MIMO) channel matrix. We have deployed a measurement platform capable of direct measurement of the MIMO wireless channel response for up to 16x16 antennas [2]. The platform has been used to collect 4x4 and 10x10 channel data at 2.4 GHz for representative scenarios. The data suggests that the bulk statistics of the channel exhibit correlated Rayleigh fading. In this paper, we show measured PDFs of the channel matrix elements, measured spatial and temporal channel correlation, and dependence of measured channel capacity on antenna polarization, antenna directivity, and the number of antennas.

2. MEASUREMENT SYSTEM CONFIGURATION

The 4x4 and 10x10 channel data were collected at 2.45-GHz, and 2.42-GHz, respectively. The center frequency was chosen to match the exact resonant frequency of the antennas. The channel was probed using 1000-bit pseudorandom binary sequences with a chip rate of 12.5-Kbps, yielding a nominal bandwidth of 25-kHz. The channel was estimated once for each complete codeword, or once every 0.08-s.

3. MEASUREMENT LOCATIONS

The measured data which is presented in this paper falls into five basic datasets. The following table lists the data sets and the transmit and receive locations. Room 484 is a central lab in our engineering building. Room 400 is a lab separated from 484 by a hallway. The transmitter was located in this hallway for certain measurements, designated as "Hall." "5 rooms" indicates that the receiver was placed at several locations in five different rooms.

The three linear antenna arrays employed were 4 element single polarization patches with $\lambda/2$ spacing (4SP), 2 element dual polarization (V/H) patches with $\lambda/2$ spacing (2DP), and 10 element monopole antennas with $\lambda/4$ spacing (10SP). Data records were each 10-s long.

This work was supported by the National Science Foundation under Wireless Initiative Grant CCR 99-79452.

Name	Xmit Loc	Recv Loc	Ant	Records
4x4(a)	RM484	5 Rooms	4SP	233
4x4(b)	Hall	RM400	2DP	165
10x10(a)	Hall	RM400	10SP	474
10x10(b)	RM484	RM400	10SP	274
10x10(c)	RM484	RM400	10SP	120

4. CHANNEL NORMALIZATION

Since the actual measured SNR varies as a function of the transmit and receive locations, some type of channel normalization is required to compare to the results. One way to consistently normalize the channel matrix (referred to as H) is to specify an average single-input single-output (SISO) SNR and scale all of the elements of each H matrix accordingly. Our average SISO SNR is defined as

$$\mathrm{SNR} = \frac{P_T/\sigma^2}{N_R N_T} \sum_{i=1}^{N_R} \sum_{j=1}^{N_T} |AH_{ij}|^2 \tag{1}$$

where P_T is the total transmit power, N_T and N_R are the number of transmit and receive antennas, and A is our normalization constant. Let receiver noise power $\sigma^2 = P_T/\mathrm{SNR}$ so that

$$A = \left(\frac{1}{N_R N_T} \sum_{i=1}^{N_R} \sum_{j=1}^{N_T} |H_{ij}|^2 \right)^{-\frac{1}{2}} . \tag{2}$$

5. CHANNEL MATRIX ELEMENT STATISTICS

This section presents measured marginal PDFs for the magnitude and phase of the elements of H. The empirical PDFs for element magnitude and phase were computed according to

$$p_m[x] = \frac{1}{N N_R N_T \Delta x} \underset{N, N_R, N_T}{\mathrm{HIST}} (|H_{ij}|, \Delta x) \tag{3}$$

$$p_a[x] = \frac{1}{N N_R N_T \Delta x} \underset{N, N_R, N_T}{\mathrm{HIST}} (\angle H_{ij}, \Delta x) \tag{4}$$

where $\mathrm{HIST}(f, \Delta x)$ represents a histogram of the function f with bins of size Δx, and N is the number of time samples. In this case histograms were computed treating each combination of time sample, transmit antenna, and receive antenna as an observation.

Figure 1 shows the PDFs for element magnitude and phase for set 4x4(a). Figure 2 shows the PDFs for set 10x10(a). The empirical PDFs for magnitude and phase are compared with the Rayleigh distribution with parameter $\sigma^2 = 0.5$ and the uniform distribution on $[-\pi, \pi]$. The agreement between the analytical and empirical PDFs is excellent. The improved fit for 10x10 data arises from more records and antennas available for averaging.

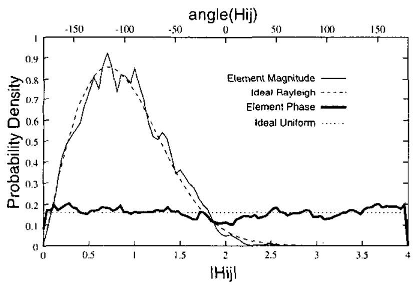

Fig. 1. Empirical PDFs for magnitude and phase of the 4x4 H matrix elements, compared with Rayleigh and uniform PDFs, respectively.

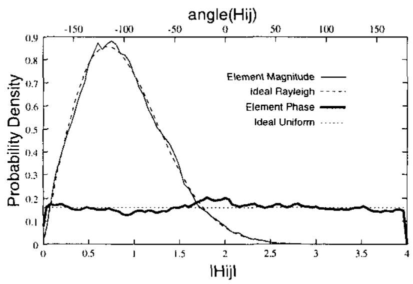

Fig. 2. Empirical PDFs for the magnitude and phase of the 10x10 H matrix elements.

6. CORRELATION FUNCTIONS

The marginal PDFs in the previous section only describe the behavior of each element of H at a single point in time, and without regard to the other H matrix elements. Due to the lack of correlation information, existing models often assume ideal cases; perfect time correlation and zero spatial correlation might be assumed, for example. The applicability of such models is suspect. This section presents a short study on the measured temporal and spatial correlation of the channel.

6.1. Channel Temporal Correlation

The indoor channel is subject to temporal drift on the order of seconds. In this paper, the temporal autocorrelation function was computed according to

$$X_k = \langle H_{ij}[n] H_{ij}^*[n+k] \rangle \tag{5}$$

where i and j are receive and transmit antenna indices, n is a time sample, k is a sample shift, and $< \cdot >$ represents an average over all combinations of transmit antenna, receive antenna, and starting time sample. The temporal correlation coefficient is then given by $\rho_k = X_k / X_0$.

Figure 3 plots the magnitude of the temporal correlation coefficient over a period of 5 seconds for each of the data sets considered.

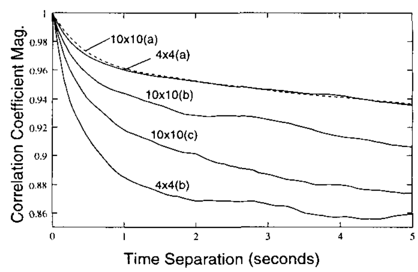

Fig. 3. Temporal correlation coefficient over a 5 second interval for all data sets.

The temporal correlation seems to exhibit an exponential decay to a "resting" correlation value, suggesting that the channel elements have fairly constant mean over the 5-s interval. This is reasonable, since the main perturbations to the channel are people walking by and doors opening and closing. These disturbances would be temporary, causing the channel to oscillate about a constant value. Over longer periods of time, the correlation might drop more substantially due to more permanent changes in the channel.

We note that the 10x10(a) and 4x4(a) data sets have nearly identical temporal correlation. These measurements were taken during periods of very low activity. Also, the data sets were quite large and represent very good statistical averages. Nearly half of the subsets in set 10x10(b) involved continuous movement of the receiver or transmitter during acquisition, which would lead to a much quicker drop in correlation. 10x10(c) and 4x4(b) were both taken during the middle of the day when activity would be higher. Also, these were the smallest data sets and might not represent good averages.

6.2. Channel Spatial Correlation

The spatial correlation of the channel is a physical mechanism which translates into H and therefore capacity. The more statistically uncorrelated the signals are at the transmit and receive antenna positions, the higher the average capacity of the channel will be. The idea of statistical correlation of receive antennas needs no explanation. Transmit correlation is less intuitive, but can be understood by considering two transmitters sending independent streams to a single receiver. Transmit correlation means the degree of correlation of the fading of the two independent streams at the single receive antenna.

We have chosen to study the spatial correlation behavior of the channel by assuming a channel correlation function which is separable at transmit and receive or,

$$R(i,j;k,\ell) = \mathrm{E}[H_{ij}H_{k\ell}^*] = R_R(i,k)R_R(j,\ell) \qquad (6)$$

with the transmit and receive correlation functions given by

$$R_T(i,j) = (1/N_R)\sum_{k=1}^{N_R}\mathrm{E}[H_{ki}H_{kj}^*] \qquad (7)$$

$$R_R(i,j) = (1/N_T)\sum_{k=1}^{N_T}\mathrm{E}[H_{ik}H_{jk}^*] \qquad (8)$$

where $\mathrm{E}[\cdot]$ is an expectation. The transmit and receive correlation functions may be computed empirically by replacing the expectation with an average over all time samples.

Figure 4 shows the shift-invariant spatial correlation coefficient at transmit and receive compared with Jake's model. This figure was created using data sets 4x4(a) and 10x10(a). For this shift-invariant case, we treat pairs of antennas with the same spacing as additional observations. For small separation, the agreement between the experimental correlation and Jake's model is very good. The disparity at higher separations may be due to non-uniform angle of arrival or insufficient data to compute the correlation statistics.

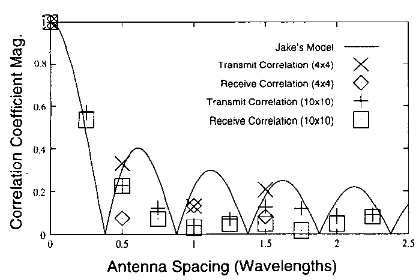

Fig. 4. Magnitude of the shift-invariant spatial correlation coefficients at transmit and receive compared with Jake's model.

7. CAPACITY

One of the most interesting channel parameters is the channel capacity, or the upper bound on achievable data rates for the channel. Capacities were computed according to the water filling solution of the channel orthogonalized by the SVD with an assumed SISO SNR of 20dB (see [3], [4]).

7.1. Polarization Dependence

The patch antennas employed were linear arrays of four dual-pol. elements. In this study, we used four transmit/receive channels (set 4x4(b)) to excite the V and H feeds on two $\lambda/2$ separated patches on each side of the link. By looking at the appropriate submatrices of H, the CCDFs (complimentary cumulative distribution functions) of capacity for various 2x2 channels can be compared.

The three basic 2x2 matrices are (1) 2 elements with same polarization (V or H), but separated by $\lambda/2$, (2) 2 elements which have orthogonal polarization and are colocated, and (3) 2 elements which have both orthogonal polarization and are separated by $\lambda/2$.

Figure 5 plots the CCDFs for a number of important cases. Two single polarization elements (SP) is the inferior case, due to substantial correlation between the elements. The next line on the graph (IID) is the capacity for a 2x2 channel matrix with independent complex Gaussian elements with unit variance, with capacity computed using Monte Carlo over 10^6 channel realizations. The capacities for the dual polarized elements (DP) and dual polarized elements with separation (DPS) are virtually identical. The fact that the dual polarized elements outperform the IID case seems extraordinary at first glance. However, it is a well-known phenomenon that coupling between the orthogonal polarizations will be small, presenting an H matrix which is nearly diagonal. The final line (DIAG) plots the case when H has iid complex Gaussian elements on the diagonal but is identically zero everywhere else (computed in a manner similar to IID). As expected, this case outperforms our dual-polarization elements which exhibit weak correlation.

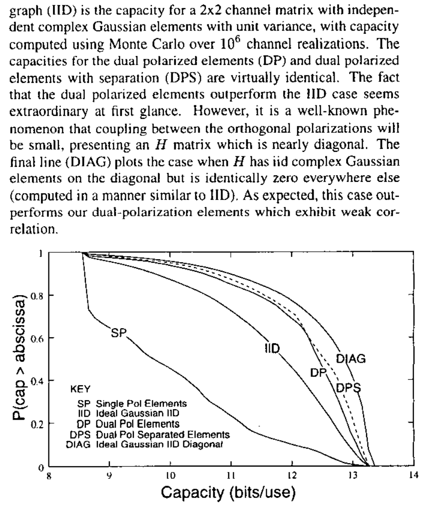

Fig. 5. CCDFs for 2x2 channels employing different types of polarization/spatial separation.

7.2. Directivity Dependence

The monopole antennas employed radiate uniformly in the plane perpendicular to the antennas. The patch antennas, on the other hand, only radiate into a half space. These two types of antennas allow the study of the effect of antenna directivity on channel capacity.

Figure 6 plots the capacity of the 4x4 channel for four patch antennas (transmit and receive) from set 4x4(a) with 4x4 subsets of the 10x10 channel for 10 monopole antennas from set 10x10(a).

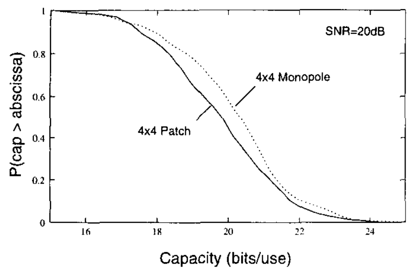

Fig. 6. Capacity CCDFs for 4x4 patches versus 4x4 Monopoles.

We note that the omnidirectional antennas (slightly) outperformed the patch antennas. This result may be somewhat misleading due to the normalization of H. It is reasonable that since the monopoles are omnidirectional, they would "see" more multipath, exhibiting higher capacity. However, the loss of multipath in the directional case may be completely compensated by the boost in SNR, allowing a higher data rate than in the omnidirectional case. This second effect is ignored since the H matrices are normalized to a specified SISO SNR. The similarity of the CCDFs suggests that even though the patch antennas only "see" a half-space, the multipath is nearly as rich as the omnidirectional case for a small number of antennas.

7.3. Dependence on Number of Antennas

Finally we looked at the dependence of capacity on the number of antennas for 2, 4, and 10 monopole transmit and receive antennas. To make a fair comparison, each array had the same total length (2.25λ). This study used set 10x10(a).

Figure 7 shows the capacity CCDFs per number of transmit and receive antennas. Also, Monte Carlo simulations were performed to obtain capacity CCDFs for channel matrices having iid complex Gaussian elements with unit variance.

We note that the agreement between the measured 2x2 and ideal 2x2 (independent Gaussian) channel is very good, since the antennas are widely separated (2.25λ). The ideal case predicts that the capacity per antennas should approach a constant as the number of antennas becomes large. Measurement shows, however, that as we pack more antennas into our array, the capacity per antenna drops, due to higher correlation between adjacent elements.

8. CONCLUSION

Wireless communications systems employing multiple antennas on both sides of the transmission link have potentially greater capacity than their single antenna counterparts. Much of the recent activity in the arena of wireless communications is focused on characterizing the MIMO channel and finding ways to exploit the increased capacity. Simple analytical models have been employed to study the channel. However, applicability of these models to complex scattering environments requires theoretical or experimental validation.

This paper has presented recently-collected MIMO wireless channel data at 2.4-GHz. The data suggests that fairly simple models may be adequate to capture bulk statistics of the indoor wireless channel. For example, the marginal PDFs of the H matrix element magnitudes and phases are nearly equivalent to Rayleigh and uniform PDFs, respectively. Also, the time correlation of channel appears to exhibit an exponential decay on the order of seconds. Further, assuming a separable form for the channel correlation function leads to transmit and receive correlation coefficients which compare very well with Jake's model. Models based on these observations may provide a very efficient starting point for simulating MIMO system performance.

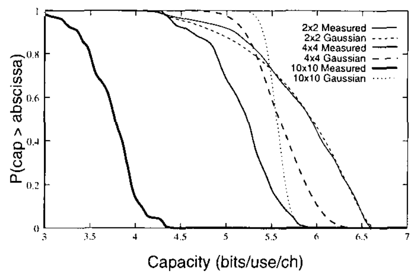

Fig. 7. Capacity CCDFs per number of antennas for transmit/receive arrays of increasing number of elements. The array length is $2.25\ \lambda$ for all cases.

9. REFERENCES

[1] G. J. Foschini and M. J. Gans, "On limits of wireless communications in a fading environment when using multiple antennas", *Wireless Personal Communications*, vol. 6, no. 3, pp. 311–335, March 1998.

[2] Jon W. Wallace and Michael A. Jensen, "A system for measuring the indoor and outdoor MIMO wireless channel response", in *2000 URSI/USNC National Radio Science Meeting Digest*, Salt Lake City, UT, July 16-21 2000.

[3] Gregory G. Rayleigh and John. M. Cioffi, "Spatio-temporal coding for wireless communication", *IEEE Transactions on Communications*, vol. 46, no. 3, pp. 357–366, March 1998.

[4] Thomas M. Cover and Joy A. Thomas, *Elements of Information Theory*, John Wiley & Sons, 1991.